DNA-Templated Biomimetic Enzyme Sheets on Carbon Nanotubes to Sensitively In Situ Detect Superoxide Anions Released from Cells

*Xiaoqing Ma, Weihua Hu, Chunxian Guo, Ling Yu, Lixia Gao, Jiale Xie, and Chang Ming Li**

Superoxide anion (O_2^-) is implicated in a wide variety of biological phenomena and oxidative stress-related diseases. The electrochemical detection of O_2^- is very attractive but relies on superoxide dismutase enzymes, thus suffering from high cost and low durability. The advances of nanoscience allows architecting while functionalizing a biomimetic sensing platform in nanoscales for high sensitivity and specificity. In this work, manganous phosphate ($Mn_3(PO_4)_2$) nanosheets, a biomimetic enzyme, are template-synthesized with DNA and further assembled on carbon nanotubes (CNTs) to form unique DNA-$Mn_3(PO_4)_2$-CNT nanocomposite sheets, of which the $Mn_3(PO_4)_2$ sheets efficiently catalyze the dismutation of O_2^- while CNTs enable fast electron transfer, thus achieving highly sensitive and specific detection of O_2^- with long-term stability. The biomimetic O_2^- sensor is further used to monitor O_2^- *in situ* released from mouse cancer cell and normal skin cell under drug stimulation, showing excellent real time quantitative detection capability. This work demonstrates a nanoscale approach to not only synthesize but also design a biomimetic enzyme for comparable performance with the natural enzyme-based biosensor while rendering much higher durability than the natural one and thus holding a great promise for broad applications in fundamental research, clinic diagnostics and screening for drug therapy effects.

1. Introduction

Primary reactive oxygen species (ROS) such as hydrogen peroxides and superoxide anion (O_2^-) exist in a wide variety of biological systems.[1–3] In particular O_2^- is implicated in various important biological phenomena such as aging, cancer development, pathogenesis of atherosclerosis and neurodegenerative diseases.[4–8] Under normal physiological conditions, the endogenous physiological concentration of O_2^- is rather low and very difficult to be detected as it rapidly disproportionates via a number of noncatalytic or/and enzymatic reaction paths. However, upon the change of physiological conditions such as occurrence of diseases, ischemia-reperfusion or hypoxia, its concentration considerably increases.[9,10] Therefore, it is of great importance to fast, reliably, sensitively and specifically detect O_2^- for pathological study, disease diagnosis and health screening.

Some methods have been employed to detect O_2^- such as ESR spin trapping, spectrophotometry, chemiluminescence and electrochemical technique,[11–14] of which the electrochemical one is very attractive due to its advantages of simplicity, selectivity, low instrument cost, real-time assay and possibility of in vivo detection. Up to date, a wide diversity of electrochemical enzyme sensors have been reported to detect O_2^- by utilizing specific enzyme catalysts such as cytochrome *c* and superoxide dismutase (SOD).[15–17] The nanomaterials-based direct electrochemistry of redox enzyme further improves the performance of O_2^- sensors.[18] Nevertheless, these enzyme-based biosensors are limited from high cost and poor long-term stability as natural enzymes are apt to be denatured and lose their biological activity in an unfavorable environment.

Synthetic biomimetic enzyme is an alternative to detect O_2^- by its catalytic dismutation of O_2^- as a low cost artificial enzyme while possessing excellent stability. Manganese was first used as an effective catalyst to provide in vivo protection against superoxide toxicity in 1982.[19] Later it has been further unveiled that only manganese phosphate ($Mn_3(PO_4)_2$) is able to catalyze the dismutation of O_2^- while free Mn^{2+} ion only stoichiometrically reacts with O_2^-.[20] An electrochemical sensor was reported to detect O_2^- by incorporating Mn^{2+} onto highly conductive TiO_2 nanoneedles with Nafion polymer as a binder,[21] but requiring potassium phosphate (K_3PO_4) in samples to

X. Ma, Prof. W. Hu, Prof. C. Guo, Prof. L. Yu, L. Gao, J. Xie, Prof. C. M. Li
Institute for Clean Energy & Advanced Materials
Southwest University
Chongqing 400715, PR China
E-mail: ecmli@swu.edu.cn
X. Ma, Prof. W. Hu, Prof. C. Guo, Prof. L. Yu, L. Gao, J. Xie, Prof. C. M. Li
Chongqing Key Laboratory for Advanced Materials and Technologies of Clean Energies
Chongqing 400715, PR China
X. Ma, Prof. W. Hu, Prof. C. Guo, Prof. L. Yu, L. Gao, J. Xie, Prof. C. M. Li
Faculty of Materials and Energy
Southwest University
Chongqing 400715, PR China

DOI: 10.1002/adfm.201401443

provide phosphate ions for catalytic dismutation, thus greatly hindering its practical applications, especially for in vivo detection. In addition its performance is much lower than that with natural SOD based sensors. This is very likely to be originated from a limited amount of Mn^{2+} and/or PO_4^{3-} ions on the electrode surface. Moreover the leakage of Mn^{2+} ions also result in decay of assay performance for questionable long-term stability.

The advances of nanoscience offers powerful tools to template or/and architect various materials for superior nanostructures and unique properties.[22–24] Herein a novel electrochemical sensor is synthesized and further architected in nanoscales by using DNA as a template to produce $Mn_3(PO_4)_2$ nanosheets ($Mn_3(PO_4)_2$), a biomimetic enzyme onto carbon nanotubes (CNTs) for sensitive in situ detection of O_2^-, in which the nanosheets with high specific surface areas and abundant active sites can effectively catalyze the dismutation of O_2^- while the highly conductive CNTs could significantly promote electron transfer between the biomimetic enzyme and the electrode, enabling in situ quantitative detection of O_2^- released from living normal and cancer cells with high sensitivity, good selectivity, fast response and long stability and thus rendering a powerful tool to explore the key role of O_2^- in various physiological and pathological processes. This approach holds a great promise for broad applications in clinic diagnostics and drug discovery.

2. Results and Discussion

The $Mn_3(PO_4)_2$ nanosheets were synthesized by using dsDNA as a unique template via a facile two-step procedure as described in the experimental part. Transmission electron microscope (TEM) images of the as prepared nanosheets in **Figure 1**a and b show a well-defined thin-layer structure with an irregular two-dimensional shape and lateral dimensions varying from 100 nm up to micrometer level, which is in line with the scanning electron microscope (SEM) image displayed in Figure 1c. X-ray diffraction pattern (Figure S1 in Supporting Information) confirms the amorphous nature of the nanosheets. Their thickness is ~15 nm as unveiled by the atom force microscope (AFM) image shown in Figure 1d. Control experiments show that in the absence of dsDNA template only nanoparticle-aggregated $Mn_3(PO_4)_2$ is formed as shown in Figure S2, indicating that dsDNA plays a pivotal role in synthesis of $Mn_3(PO_4)_2$ nanosheets as schematically described in **Scheme 1**. The dsDNA may not split to ssDNA at a mild high temperature but should be stretched in a heated solution without tangling with each other. It is proposed that the formation of the sheet biomimetic enzyme starts with Mn^{2+} ions electrostatically interacting with the negatively charged phosphate backbone of dsDNA in the solution followed by facilitating a nucleation to grow $Mn_3(PO_4)_2$ nanoparticles by adding potassium phosphate (K_3PO_4) due to the low solubility of $Mn_3(PO_4)_2$ for its deposition in the solution. After adding K_3PO_4 under stirring for 10 min, necklace-like DNA-$Mn_3(PO_4)_2$ chains are formed (Figure S3 in Supporting Information). The continuous growth for 1 hour under stirring could connect the necklace with each other, finally resulting in well-defined assembled DNA-$Mn_3(PO_4)_2$ nanosheets.

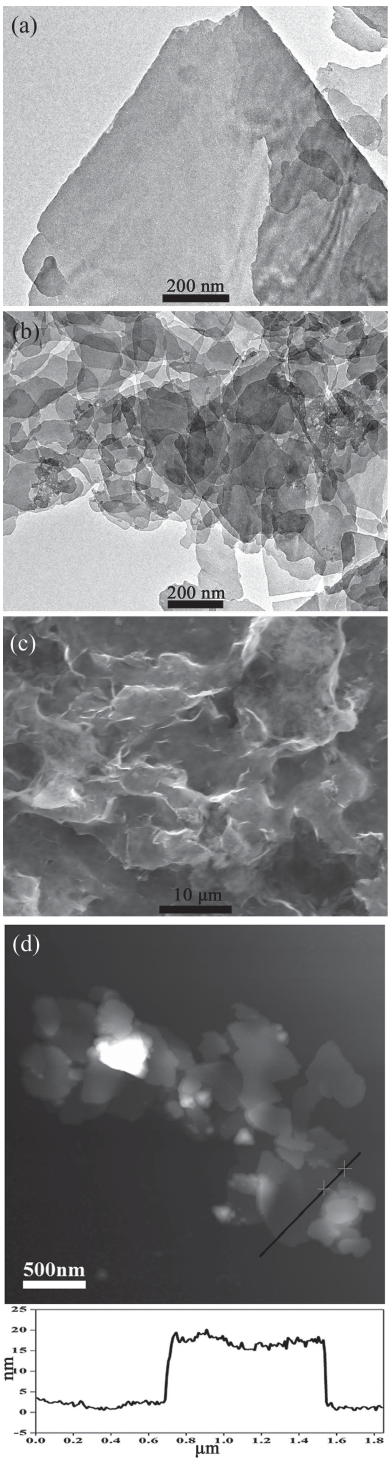

Figure 1. Material characterization of DNA-$Mn_3(PO_4)_2$ nanosheets (a), TEM images (b), SEM image (c) and AFM image (d).

The prepared DNA-$Mn_3(PO_4)_2$ nanosheets are further casted onto a CNTs (multi-walled, the TEM images in Figure S4) modified glassy carbon electrode to construct a DNA-$Mn_3(PO_4)_2$@CNTs@GC electrode, on which the electrocatalytic behavior towards O_2^- reaction is studied using cyclic voltammetry (CV).

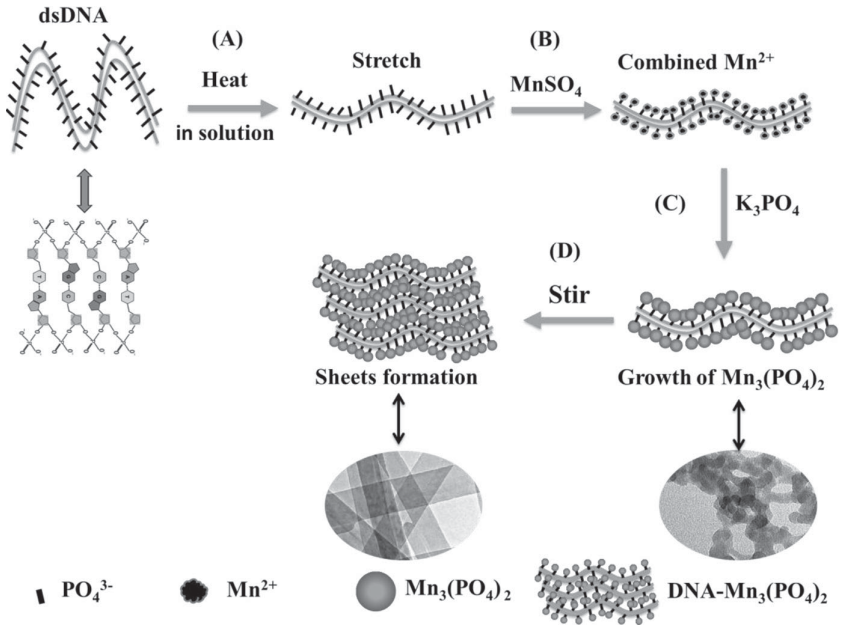

Scheme 1. Schematic illustration of the formation of DNA-$Mn_3(PO_4)_2$ nanosheets : (A) heating the double-stranded DNA at 60 °C; (B) electrostatically attaching manganous ions (?) onto the phosphate group of DNA; (C) nucleating and deposition of manganese phosphate nanoparticles on DNA; (D) growing the biomimetic enzymes DNA-$Mn_3(PO_4)_2$ nanosheets by stirring.

The prepared electrode shows a sharp oxidative peak around 0.6 V and a reductive wave around 0.4 V (date shown in Figure S5a) in the absence of O_2^-, which can be assigned to the electrochemical transformation between Mn(II) and Mn(III) species. In the presence O_2^- both oxidative and reductive currents evidently increase (Figure S5a), which is consistent with the previous report.[21] During the redox process a O_2^- oxidizes the Mn^{2+} to generate MnO_2^+ and H_2O_2 while another O_2^- simultaneously reduces the MnO_2^+ to produce Mn^{2+} and O_2, resulting in increased redox current.[21] The CV results clearly confirm that the catalytic activity of the biomimetic enzyme $Mn_3(PO_4)_2$ towards the dismutation of O_2^- is retained in the nanosheets and the electron transfer between $Mn_3(PO_4)_2$ and the underlying electrode is efficiently mediated by the conductive CNTs, indicating the DNA-$Mn_3(PO_4)_2$@CNTs@GC electrode is an efficient biosensor towards O_2^- detection.

To demonstrate the advantage of the DNA-$Mn_3(PO_4)_2$ nanosheets for electrochemical O_2^- detection, $Mn_3(PO_4)_2$ nanoparticles and DNA-Mn^{2+} complex formed without further addition of K_3PO_4 to form sheets were casted on CNT-modified GC electrodes, respectively for comparison. The measured CVs show that the DNA-Mn^{2+}@CNTs@GC electrode has similar redox pair as DNA-$Mn_3(PO_4)_2$ @ CNTs @ GC and the addition of O_2^- induces increased currents shown in Figure S5b, suggesting successful incorporation of Mn^{2+} ions in the dsDNA. However, both the currents and current increase upon O_2^- addition are much smaller than that on DNA-$Mn_3(PO_4)_2$@CNTs@GC electrode (data shown in **Figure 2**), reflecting much poorer sensitivity towards detection of O_2^-. It can be very reasonably concluded that the DNA-Mn^{2+}@CNTs@GC misses the formation step of $Mn_3(PO_4)_2$ and thus could not have as many Mn^{2+} reaction centers for dismutation of O_2^- as that of $Mn_3(PO_4)_2$ based nanosheets. The $Mn_3(PO_4)_2$@CNTs@GC also shows poor biomimetic electrocatalytic performance (also in Figure S5c), suggesting that aggregated $Mn_3(PO_4)_2$ nanoparticles cannot expose as many Mn^{2+} reaction center as that of the nanosheet biomimetic enzyme for O_2^- detection. The reaction mechanism is depicted in **Scheme 2**. These comparison unambiguously not only unveils the advantages of DNA-$Mn_3(PO_4)_2$ nanosheets for O_2^- detection, but also further proving the critical role of dsDNA in formation of the biomimetic enzyme.

CNTs are also an important component in the architecture of DNA-$Mn_3(PO_4)_2$@CNTs@GC for sensitive electrochemical

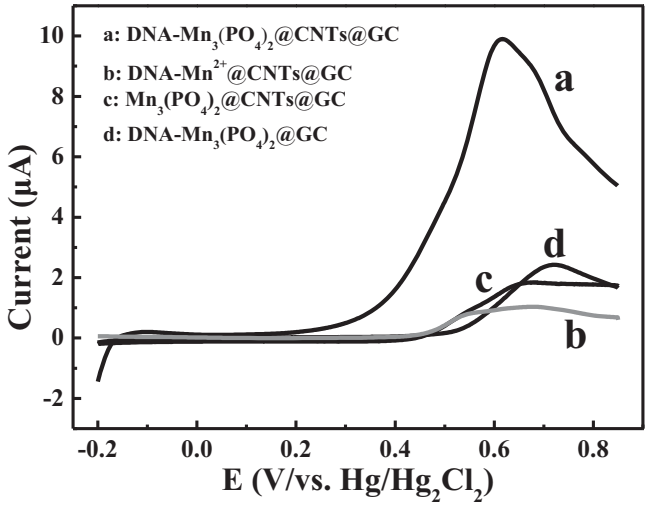

Figure 2. Voltmmaograms obtained at different modified GCE electrodes in 0.01M PBS (pH = 7.0) in the presence of 1 μM O_2^- (black lines), potential scan rate: 50 mV s^{-1}. (a) DNA-$Mn_3(PO_4)_2$@CNTs@GC, (b) DNA-Mn^{2+}@CNTs@GC, (c) $Mn_3(PO_4)_2$@CNTs@GC, (d) DNA-$Mn_3(PO_4)_2$@GC. All the voltammograms presented were background subtracted.

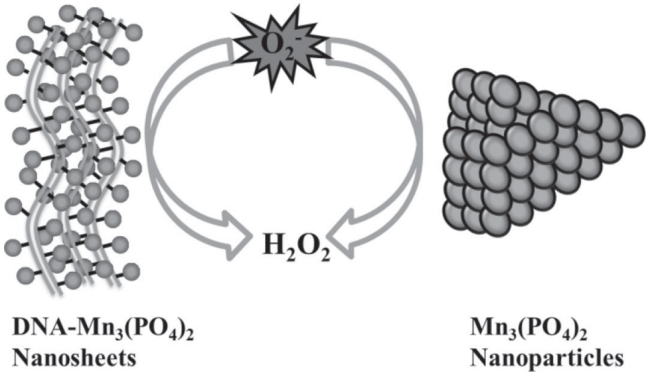

Scheme 2. Schematic illustration of the reaction mechanism of sensing O_2^- on DNA-$Mn_3(PO_4)_2$ nanosheets and $Mn_3(PO_4)_2$ nanoparticles.

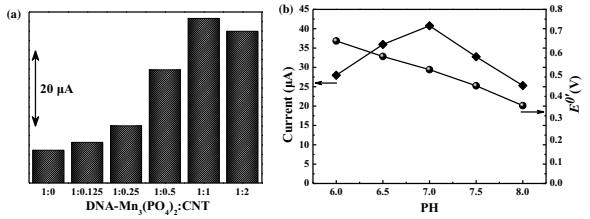

Figure 3. Quantity effect and PH effect: (a) Peak current of different ratio of DNA-$Mn_3(PO_4)_2$:CNTs film with 1 μM O_2^-. (b) Relationship between the formal potential (E_0') (blue Y-axis) and the current response (black Y-axis) of DNA-$Mn_3(PO_4)_2$@CNTs@GC biosensor in 0.01M PBS and PH values.

detection of O_2^-. As shown in Figure S5d much weaker redox currents are obtained on the DNA-$Mn_3(PO_4)_2$@GC electrode without CNT modification than that of the CNT-modified biomimetic enzyme sheet; the current increase is also much lower upon addition of a same concentration of O_2^- (only one-fifth of that on DNA-$Mn_3(PO_4)_2$@CNTs@GC. This result further clearly implies that CNTs efficiently improve the electron transfer between $Mn_3(PO_4)_2$ biomimetic enzyme and the GC electrode towards O_2^- detection. It has been reported that the DNA molecules possess high affinity to the graphitic carbon such as CNTs due to the strong π–π stacking between the atomic plane of graphite and the nucleobases.[25] In such a way the $Mn_3(PO_4)_2$ biomimetic enzyme nanosheets can closely contact CNTs to facilitate the electron transfer. On the other hand without DNA-CNT interaction in $Mn_3(PO_4)_2$@CNTs@GC only a small fraction of $Mn_3(PO_4)_2$ nanoparticles in close proximity of CNTs can perform electron transfer with the underlying electrode, resulting in weak response for O_2^- detection.

The optimization results obtained with adjustment of the ratio of DNA-$Mn_3(PO_4)_2$ nanosheets to CNTs further prove the important role of CNTs for the performance of DNA-$Mn_3(PO_4)_2$@CNTs@GC electrodes. As shown in **Figure 3**a the current response towards detection of O_2^- for DNA-$Mn_3(PO_4)_2$@CNTs@GC electrode increases with the increase of CNT amount until reaching a maximum at a weight ratio of 1:1 of CNT to DNA-$Mn_3(PO_4)_2$. Further increase is detrimental, indicating that CNTs facilitate the electron transfer as mediators by electrically connecting $Mn_3(PO_4)_2$ with the underlying electrode to enhance the electron transfer. However excess CNTs could disturb the close electronic communication of $Mn_3(PO_4)_2$ nanosheets with embedded GC electrode.

The pH effect on the electrochemical behavior of the DNA-$Mn_3(PO_4)_2$@CNTs@GC electrode was investigated as shown in Figure 3b. The CVs of the electrode in solutions with different pH values are shown in Figure S6. It is found that the formal potential (*E0'*) is pH-dependent, showing a linear decrease on increasing pH from 6.0 to 8.0 with a slope of ~100 mV/pH, which is consistent with the previous observations.[21,26,27] Meanwhile the highest current response towards detection of O_2^- among all investigated pH values is observed in a neutral solution (pH = 7). Moreover, in a pH range over 6.5–7.5 the current responses are consistent with small variations, enabling reliable detection of O_2^- in a neutral solution.

The amperometric response of DNA-$Mn_3(PO_4)_2$@CNTs@GC electrode to successive concentration changes of O_2^- is recorded at an applied potential of 700 mV *vs.* Hg/Hg_2Cl_2/saturated KCl (**Figure 4**a, black line). The potential is selected in such a way that it is around the middle point of the diffusion controlled plateau current region in the steady-state polarization curves (data not shown) for reliable detections in case of electrode deterioration to cause a reaction potential shift. Well-defined steady-state currents are obtained and increase stepwise with successive additions of O_2^- in a range of nanomolar (nM) to micromolar (μM). As low as 10 nM O_2^- is able to arouse a sensitive and swift current response on the electrode as displayed in inset 1 in Figure 4a. The measured response time is less than 5 s in response to a step injection of O_2^-. A relative standard deviation of 0.4% for six successive assays of 57.5 nM O_2^- is achieved, indicating excellent reproducibility of the biomimetic enzyme sensor. In contrast, without CNTs the DNA-$Mn_3(PO_4)_2$@GC electrode shows very weak current response with high noise towards detection of O_2^- (red line and its enlarged one in inset 2 of Figure 4a), which is in agreement with the CV observations shown in Figure 2.

The amperometric current of the DNA-$Mn_3(PO_4)_2$@CNTs@GC biomimetic enzyme sensor has good linear relation to the O_2^- concentrations with a correlation coefficient of 0.999 in a range of 10^{-8} to 7×10^{-4} M (Figure 4b), which well meets the concentration requirement of O_2^- detection in normal physiological conditions (~10^{-7} M) and morbid status (10^{-4}–10^{-3} M).[21] The sensitivity is 6.55 μA μM^{-1} with a detection limit of ~3.3 nM based on a signal-to-noise ratio of 3:1. The performance is much superior to that obtained on previously reported $Mn_3(PO_4)_2$ biomimetic enzyme sensors in terms of sensitivity, detection limit, response time and dynamic range and thus can be used to in situ or online tracking of O_2^- in biological systems.[21]

The specificity is always an important issue in monitoring O_2^- in biological systems. Various coexisting biological compounds may result in false signals. Among the interferences hydrogen peroxide (H_2O_2) and ascorbic acid (AA) are particularly serious interferences perplexing the electrochemical detection of O_2^- as they widely exist in biological systems and possess electrochemical oxidative activity. The detection specificity of the biomimetic enzyme sensor is investigated as in Figure 4c shows that the addition of commonly existed interferences including H_2O_2, AA, Na^+, K^+, NO_3^-, Cl^- and dopamine (DA) only results in negligible current response, showing excellent specificity of the CNT@DNA-$Mn_3(PO_4)_2$@GC electrode for O_2^- detection without the disturbance from these interferences. It is worthy of a note that in comparison to 57.5 nM O_2^- as high as 1 μM of H_2O_2 only produces 2% current response and 10 μM of AA only arouses a 3.5% current response as in Figure 4d, both of which are negligible and do not significantly disturb the O_2^- detection. The response current for O_2^- recorded with the CNT@DNA-$Mn_3(PO_4)_2$@GC electrode daily has almost no changes throughout at least three weeks, thus also showing exceptional reproducibility.

The unique biomimetic enzyme sensor was further used to *in situ* detect O_2^- released from two mouse skin cell lines including B16-F10 melanoma skin cancer cells and JB6-C30 normal skin cells, respectively. The inset images of **Figure 5**a and b display the microscope images of B16-F10 and JB6-C30

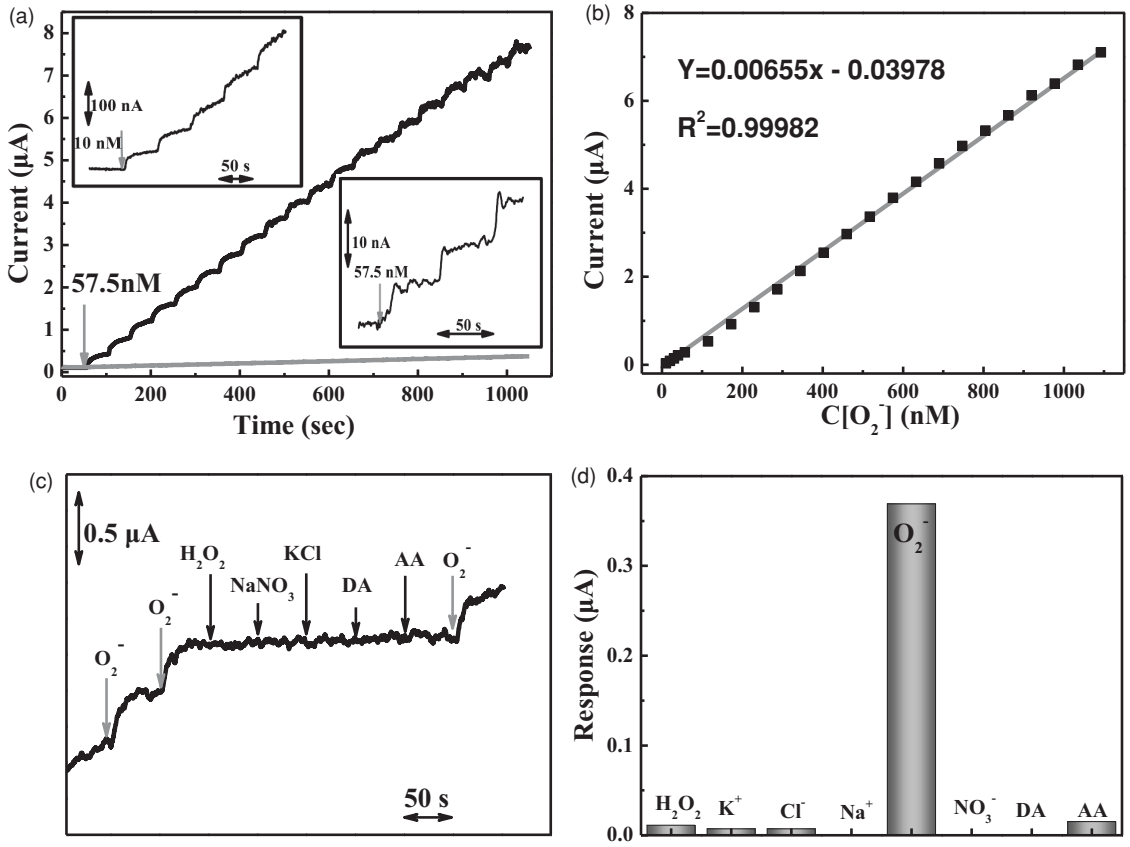

Figure 4. Typical amperometric responses (a) of DNA-$Mn_3(PO_4)_2$@CNTs@GC film and DNA-$Mn_3(PO_4)_2$ film (inset of panes are amperometric responses with low concentrations of DNA-$Mn_3(PO_4)_2$@CNTs@GC (1) and expansion curve chronoamperometry corresponding to the red curve (2)) and calibration plot of steady-state currents (b) of DNA-$Mn_3(PO_4)_2$@CNTs@GC to successive additions of 10 nM and 57.5 nM O_2^- at applied potentials of 700 mV versus Hg/Hg_2Cl_2 in 10 mol PBS (pH 7.0). Current responses (c) and histogram profile (d) of DNA-$Mn_3(PO_4)_2$@CNTs@GC for the assaying of O_2^- against the diverse interferes. The response obtained on the addition of 10 μM interferes and 57.5 nM O_2^-. The solutions were stirred with a magnetic stirrer at a suitable speed.

cells at a same density of 4×10^5 cells mL^{-1}, respectively. As shown in Figure 5a the sensor in the B16-F10 skin cancer cell suspension shows a significantly increased current response at 700 mV (versus Hg/Hg_2Cl_2) upon addition of 1.0 g L^{-1} Zymosan, an anticancer drug, suggesting significant release of O_2^- stimulated by the drug. According to the calibration curve in Figure 4a each B16-F10 skin cancer cell releases 0.051 pmol O_2^- upon the Zymosan stimulation. Increasing the drug concentration to 2.0 g L^{-1} produces a two-fold current response as the drug induces the production and release of O_2^- in a dose-dependent manner.[28] When 250 U mL^{-1} (SOD), an enzyme often as a scavenger to effectively eliminate O_2^- is injected together with 1.0 g L^{-1} Zymosan into the suspension, the current maintains at the background level without any observable current step, indicating effective elimination of O_2^- by the SOD enzyme. Control experiments show that no current obtained in the culture medium upon the addition either Zymosan or Zymosan-SOD mixture, confirming that the current responses are attributed to the drug induced O_2^- release from B16-F10 skin cancer cells. Similar results are observed for the JB6-C30 normal skin cells; however the current step intensity obtained with JB6-C30 normal skin cells is much weaker (ca. 10%) than that with B16-F10 skin cancer cells, indicating less O_2^- released by JB6-C30 cells upon the same drug stimulation (Figure 5c). The amount of O_2^- released by total cells and a single cell also calculated as summarized in **Table 1**. Another interesting difference between these two kinds of cells is that the current produced from B16-F10 skin cancer cells fast decays to the baseline level in 60 s while that for JB6-C30 cells is quite stable, possibly hinting different paths of two kinds of cells to release O_2^- or to eliminate the O_2^- stress. The investigation to understand the different mechanisms are still undergoing in our lab.

3. Conclusion

A novel O_2^- biosensor based on CNTs-supported DNA-$Mn_3(PO_4)_2$ nanosheets has been successfully developed and the formation mechanism of the biomimetic enzyme sheets is proposed. The unique properties of the nanosheets and rationally designed sensor architecture offer high sensitivity, excellent specificity, good reproducibility, long-term stability and fast response time towards detection of O_2^-. *In situ* monitoring the O_2^- released from mouse cancer skin cells and normal skin cells under drug stimulation is accomplished

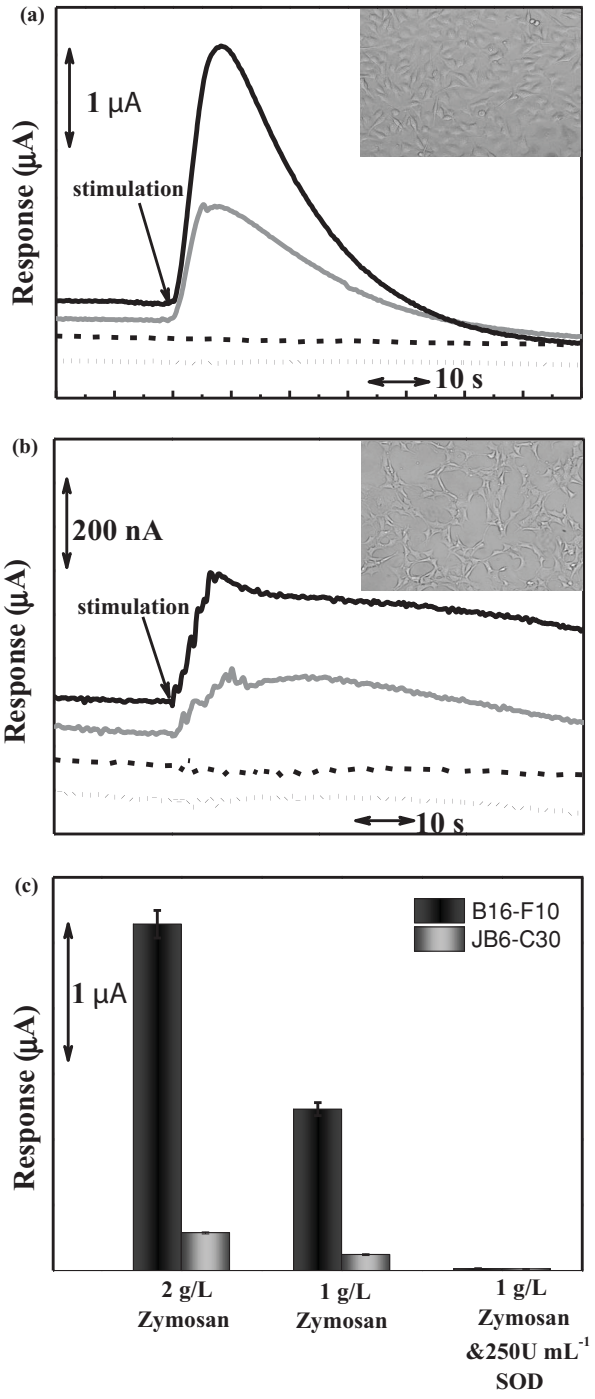

Figure 5. Electrochemical response of DNA-$Mn_3(PO_4)_2$@CNTs@GC toward mouse skin cells. (a) B16-F10 melanoma skin cancer cells and (b) JB6-C30 normal skin cells (inset of the cell images with the density of 4×105) are the cell response obtained at an applied potential of 700 mV under different stimulate. The red lines (with cultured cells) and blue lines (with cultured cells) represent the injection 2 g/L Zymosan and 1 g/L Zymosan, respectively. The green (with cultured cells) and purple lines (without cultured cells) are distinguished under the injection 1 g/L Zymosan& 250 U mL^{-1} SOD. The drug was added at the time indicated by the arrow. (c) The blue and red bars correspond to the current response of the cells after the addition of different drugs.

Table 1. Current response and amount O_2^- released by B16-F10 melanoma skin cancer cells and JB6-C30 normal skin cells under injection of different drugs.

Cell lines	Stimulation	Current [μA]	Total amount of O_2^- realeased [nmol]	O_2^- realeased by a cell [pmol]
JB6-C30	2 g/L Zymosan	0.272	41.5	0.052
	1 g/L Zymosan	0.12	18.3	0.023
	1 g/L Zymosan & 250 U/mL SOD	0.015	2.3	0.0029
B16-F10	2 g/LZymosan	2.677	408.7	0.51
	1 g/L Zymosan	1.189	181.5	0.23
	1 g/L Zymosan & 250 U/mL SOD	0.01	1.5	0.0019

by this biosensor, showing great capability for real time and sensitively quantitative detection. This work demonstrates an approach in nanoscales to not only synthesize but also to architect a biomimetic enzyme for comparable performance with the natural-enzyme based biosensor while rendering much higher durability than the natural one and thus holding a great promise for broad applications in fundamental research, clinic diagnostics and screening for drug therapy effects.

4. Experimental Section

Materials: Concentrated sulfuric acid and concentrated nitric acid were purchased from East Sichuan Chemical Industry (Group) Co., Ltd. (Chongqing, China) and used as received. Phosphate buffer solution (PBS, 10 mmol) with PH 7.0 was prepared by adjusting the standard PBS (0.01 M, PH 7.4) with PH meter. The Nafion solution purchased from Sigma-Aldrich was diluted to 5% with pure ethanol. The other chemicals were purchased from Sigma-Aldrich and used without further purification unless otherwise specified. All solutions were prepared using deionized Millipore-Q water (18 MΩ cm) and were deaerated with high purity nitrogen before experiments. All electrochemical experiments were carried out at room temperature.

Surface Modification of Multiwalled Carbon Nanotube (MWCNT): 1g of MWCNT and 1:1 volume ratio of concentrated sulfuric acid (75 mL) and concentrated nitric acid (75 mL) were placed in a 500 mL round-bottom flask followed by constantly stirring at 120 °C under reflux of water in an oil bath for 4–6 h. Then the acid solution was centrifuged at 12 000 r/min and washed until the supernatant reached neutral. The product was dried in an oven at 100 °C for ~12 h. The as-prepared functioned MWCNT dispersion was used for characterizations and experiments.

Synthesis of DNA-$Mn_3(PO_4)_2$: DNA-$Mn_3(PO_4)_2$ was prepared mainly via self-assembled Mn ions to DNA phosphate groups. 2.1 mg double-stranded DNA and 0.01 mol $MnSO_4$ solution added under constant stirring and heating. After about ten minutes 0.01 mol K_3PO_4 solution were injected into the mixture under stirring. The solution became transparent after one hour and Mn ions assembled onto DNA successfully. The obtained solution was centrifuged at 9000 r/min for 10 minutes and washed with distilled water several times. The as-prepared DNA-$Mn_3(PO_4)_2$ was dispersed in distilled water for further experiments.

Preparation of DNA-$Mn_3(PO_4)_2$@CNTs@GC: Glassy carbon electrode (GCE, d = 3 mm) was polished with 0.3 mm and 0.05 mm alumina slurry successively to a smooth and bright surface followed by

sonication in water and absolute ethanol for 30 s, respectively and then dried at room temperature under purged nitrogen. The electrodes were then electrochemically characterize by potential cycling in KCl containing solution 5 mmol $K_3[Fe(CN)_6]$ in a potential range over –0.1–0.6 V at a scan rate of 50 mV s^{-1} until a typical cyclic voltammogram (less than 80 mV peak potential differences) characteristic of a clean GCE electrode was obtained. The CNT-modified GCE was prepared by dropping 4 μL of CNT solutions on the electrode surface and drying at room temperature about 2 h. Then mixing DNA-$Mn_3(PO_4)_2$ and 5% Nafion solution at a ratio of 1:1 and coating the blend, the biomimetic enzyme DNA-$Mn_3(PO_4)_2$ onto the CNTs by dropping the blend. The as-prepared DNA-$Mn_3(PO_4)_2$@CNTs@GC was used in further experiments.

Apparatus and Characterization: All electrochemical measurements are performed in a three-electrode system using CHI-660B electrochemical station (CH Instruments). A platinum wire and KCl saturated Hg/Hg_2Cl_2 electrode were used as the counter and reference electrodes, respectively, while the modified glassy carbon electrode (GCE) was applied as the working electrode. PBS was used as the electrolyte for all the electrochemical measure except cell detection. The morphologies were investigated by scanning electron microscopy (SEM, JSM-6510LV, Japan). The nanosheets of DNA-$Mn_3(PO_4)_2$ were characterized by transmission electron microscopy (TEM, JEM-2100F, Japan). Cells images and cell cultures were acquired with an inverted microscope (IX-71, Olympus Corp, Japan). The O_2^- solutions were prepared by the addition of KO_2 solid powder to PBS (N_2 saturated). The concentration of O_2^- was determined by recording the reduction of ferri cytochrome *c* spectrophotometrically and using the extinction coefficient (21.1 mM^{-1} cm^{-1}) of ferrocytochrome *c* at 550 nm.[29] The date acquired with UV–visible spectrophotometer (Daojing UV-2450).

Cell Cultures. JB6-C30(mouse skin cancer cells)and B16-F10(mouse skin normal cells)cell lines were obtained from Chongqing University and Chongqing Medical University (Chongqing, China), respectively and cultured in a humidified incubator (95% air with 5% CO_2) at 37 °C. The cells grown in Dulbecco's Modified Eagle's Medium (DMEM) (Cellgro, USA) supplemented with 10% heat inactivated fetal bovine serum (Cellgro, USA), 1 mol L^{-1} glutamine (Beijing Dingguo Changsheng Biotech CO. LTD, China) and 50 U mL^{-1} penicillin/streptomycin (Cellgro, USA). The cell density applied to our experiments was the average cell number counted from 10 different areas of 1.8 mm^2 on three samples through inverted microscopy (IX-71, Olympus Corp, Japan).

In situ Detection of Extracellular O_2^-: For the detection of O_2^- released from living cells 2 mL DMEM medium solution (with or without living cells) was used for real sample measurements and was mildly stirred for O_2^- uniformly distributed in whole solution for accurate measurements. A Pipette (volume range from 10 μL to 100 μL) was used to inject Zymosan and (SOD). Amperometric response curves were recorded by CHI-660B electrochemical station at applied potential of 700 mV (versus Hg/Hg_2Cl_2).

Supporting Information

Supporting Information is available from the Wiley Online Library or from the author.

Acknowledgements

We would like to gratefully acknowledge the financial support from the 973 program of China (No. 2013CB127804), National Natural Science Foundation of China (No. 21205098, 21273173), Fundamental Research Funds for the Central Universities (XDJK2012C049), Chongqing Key Laboratory for Advanced Materials and Technologies of Clean Energies, Start-up grant under SWU111071 from Southwest University, Chongqing Engineering Research Center for Rapid Diagnosis of Dread Disease and Chongqing development and reform commission.

Received: May 4, 2014
Revised: May 31, 2014
Published online: July 17, 2014

[1] J. K. Andersen, *Nature Med.* **2004**, *10 Suppl*, S18.
[2] C. X. Guo, X. T. Zheng, Z. S. Lu, X. W. Lou, C. M. Li, *Adv. Mater.* **2010**, *22*, 5164.
[3] X. T. Zheng, W. Hu, H. Wang, H. Yang, W. Zhou, C. M. Li, *Biosens. Bioelectron.* **2011**, *26*, 4484.
[4] J. E. Klaunig, L. M. Kamendulis, *Annu. Rev. Pharmacol. Toxicol.* **2004**, *44*, 239.
[5] E. D. Hall, J. M. Braughler, *Free Radical Biol. Med.* **1989**, *6*, 303.
[6] A. Vanella, C. Di Giacomo, V. Sorrenti, A. Russo, C. Castorina, A. Campisi, M. Renis, J. Perez-Polo, *Neurochem. Res.* **1993**, *18*, 1337.
[7] R. A. Floyd, *FASEB J.* **1990**, *4*, 2587.
[8] B. N. Ames, M. K. Shigenaga, T. M. Hagen, *Proc. Natl. Acad. Sci. USA* **1993**, *90*, 7915.
[9] H. A. Kontos, E. P. Wei, *J. Neurosurg.* **1986**, *64*, 803.
[10] M. Y. T. Globus, O. Alonso, W. D. Dietrich, R. Busto, M. D. Ginsberg, *J. Neurochem.* **1995**, *65*, 1704.
[11] J. L. Zweier, J. T. Flaherty, M. L. Weisfeldt, *Proc. Natl. Acad. Sci. USA* **1987**, *84*, 1404.
[12] Y. Ohara, T. E. Peterson, D. G. Harrison, *J. Clin. Invest.* **1993**, *91*, 2546.
[13] J. Vasquez-Vivar, B. Kalyanaraman, P. Martasek, N. Hogg, B. S. S. Masters, H. Karoui, P. Tordo, K. A. Pritchard, *Proc. Natl. Acad. Sci. USA* **1998**, *95*, 9220.
[14] T. Ohyashiki, M. Nunomura, T. Katoh, *Biochim. Biophys. Acta-Biomembr.* **1999**, *1421*, 131.
[15] C. J. McNeil, K. R. Greenough, P. A. Weeks, C. H. Self, J. M. Cooper, *Free Radic. Res. Commun.* **1992**, *17*, 399.
[16] V. Lvovich, A. Scheeline, *Analyti. Chem.* **1997**, *69*, 454.
[17] J. Chen, U. Wollenberger, F. Lisdat, B. X. Ge, F. W. Scheller, *Sens. Actuat. B-Chem.* **2000**, *70*, 115.
[18] Y. Tian, L. Mao, T. Okajima, T. Ohsaka, *Analyt. Chem.* **2002**, *74*, 2428.
[19] F. S. Archibald, I. Fridovich, *Arch. Biochem. Biophys.* **1982**, *214*, 452.
[20] K. Barnese, E. B. Gralla, D. E. Cabelli, J. S. Valentine, *J. Am. Chem. Soc.* **2008**, *130*, 4604.
[21] Y Luo, Y. Tian, Q. Rui, *Chem. Commun.* **2009**, 3014–6.
[22] C. X. Guo, S. R. Ng, S. Y. Khoo, X. Zheng, P. Chen, C. M. Li, *ACS Nano* **2012**, *6*, 6944.
[23] C. X. Guo, Y. Q. Shen, Z. L. Dong, X. D. Chen, X. W. Lou, C. M. Li, *Energ. Environmental Sci.* **2012**, *5*, 6919.
[24] L. Y. Zhang, C. X. Guo, Z. Cui, J. Guo, Z. Dong, C. M. Li, *Chemistry* **2012**, *18*, 15693.
[25] A. N. Enyashin, S. Gemming, G. Seifert, *Nanotechnology* **2007**, *18*, 245702.
[26] H. A. Azab, L. Banci, M. Borsari, C. Luchinat, M. Sola, M. S. Viezzoli, *Inorg. Chem.* **1992**, *31*, 4649.
[27] R. N. Iyer, W. E. Schmidt, *Bioelectrochem. Bioenerg.* **1992**, *27*, 393.
[28] Q. Y. Lin, L. J. Jin, Z. H. Cao, Y. N. Lu, H. Y. Xue, Y. P. Xu, *Phytother. Res.* **2008**, *22*, 740.
[29] J. M. McCord, I. Fridovic, *J. Biol. Chem.* **1969**, *244*, 6049.